PROCEEDINGS OF SCIENCE

# Precision hyperon physics at $J/\psi$ and $\psi'$ factories

**Andrzej Kupść**[a,b,*]

[a] *Department of Physics and Astronomy, Uppsala University, Box 516, SE-75120 Uppsala, Sweden*

[b] *Department of Fundamental Research, National Centre for Nuclear Research, Pasteura 7, 02-093 Warsaw, Poland*

*E-mail:* Andrzej.Kupsc@physics.uu.se

A novel multidimensional method to study hyperon and antihyperon decays and to search for a direct CP-violation signal is presented. The method uses spin polarization and entanglement of baryon–antibaryon pairs produced in electron–positron annihilation at the $J/\psi$ and $\psi'$ resonances. The method was applied in a series of proof-of-concept analyses at BESIII. The helicity amplitudes describing electron–positron annihilation into $\Lambda\overline{\Lambda}$, $\Sigma^+\overline{\Sigma}^-$, $\Xi^-\overline{\Xi}^+$ and $\Omega^-\overline{\Omega}^+$ pairs at $J/\psi$ or $\psi'$ were determined. A significant transverse polarization of the (anti)hyperons in $J/\psi$ and $\psi'$ decays was observed and spin of the $\Omega^-$ baryon was determined in a model independent way using the reaction properties. The asymmetry parameters of the main (anti)hyperon decay modes, the non-leptonic two-body decays, were precisely measured. The result for the asymmetry parameter $\alpha_\Lambda$ in $\Lambda \to p\pi^-$ revises by 17% the value used for nearly 50 years in all analyses of $\Lambda$ polarization. Additionally, in the sequential weak decays $\Xi^- \to \Lambda\pi^-$ and $\Omega^- \to \Lambda K^-$ the spin rotation parameter was measured.

A comparison of the hyperon and antihyperon decay parameters allows for tests of direct CP-symmetry violation, that are complementary to the $\epsilon'/\epsilon$ measurement in kaon decays. Of special importance are the new results on $e^+e^- \to J/\psi \to \Xi^-\overline{\Xi}^+$, where the final-state interaction and weak-phase difference are disentangled. Prospects of future measurements at Super Charm-Tau Factories are discussed with the emphasis on the impact of the longitudinal polarization of the electron beams on the precision of the CP-violation tests.

**** 10th International Workshop on Charm Physics (CHARM2020), ****
**** 31 May - 4 June, 2021 ****
**** Mexico City, Mexico - Online ****

*Speaker





PoS(CHARM2020)009

*Dedication*

*Simon was the life and soul of our community and a dear friend for many of us. He was also the ultimate light meson physics authority for me ever since I first met him in his and Boris Shwartz office in February* 1996.

## 1. Introduction

The well-defined and simple initial state makes a baryon–antibaryon pair production at electron–positron colliders an ideal system to investigate the baryon properties and to test fundamental symmetries. Not only the spin orientations of the baryon and antibaryon are correlated, but due to the strong interactions in the final state, the transition amplitudes to the respective spin states can acquire relative phases leading to polarization of the baryons. The baryon–antibaryon pair production in the single-photon electron–positron annihilation is related to the time-like elastic baryon form factors. The formalism of such processes is well known for baryons with spin-1/2 [1–5]. The cross sections for the non-resonant annihilation are low and the available data sets do not allow for precision studies of baryon decays. However, as it was shown in Ref. [6], the same formalism is valid for experiments at the centre-of-mass (c.m.) energies corresponding to the $J/\psi$ and $\psi'$ resonances. Given relatively large branching fractions of the $J/\psi \to B\overline{B}$ processes, $O(10^{-3})$, and the huge data sample of $10^{10}$ $J/\psi$ events collected at BESIII, multidimensional analyses to determine decay properties of hyperons and antihyperons are now feasible.

This contribution is organised as follows: weak non-leptonic decays of hyperons are described in Sec. 2, direct CP-violation in $|\Delta S| = 1$ transitions in kaons and hyperons is discussed in Sec. 3. Formalism to describe baryon–antibaryon pair production in electron–positron annihilation is summarised in Sec. 4 and the BESIII results are reported in Sec. 5. The implications of results are discussed in Sec. 6 and the outlook for measurements at Super Charm-Tau Factories (SCTF) with polarized electron beams is in Sec. 7.

## 2. Hyperon weak hadronic decays

The main decay modes of the ground-state hyperons are weak-$|\Delta S| = 1$ transitions into a baryon and a pseudoscalar meson. Some of the processes are listed in Table. 1, where the Particle Data Group (PDG) averages before 2018 [7] and the most recent results are reported. Historically, they provided the crucial information for establishing the patterns of parity violation in weak decays [14]. Nowadays, they are used in searches of CP-symmetry violation signals in baryon sector and to determine spin polarization in hadronic reactions involving hyperons.

For a weak decay $D$ of a spin-1/2 baryon $B$ to a spin-1/2 baryon $b$ and a pion, $D(B \to b\pi)$, like $\Lambda \to p\pi^-$ or $\Xi^- \to \Lambda\pi^-$, the parity-even amplitude leads to the final state in the $p$-wave and parity-odd amplitude leads to the final state in the $s$-wave. The two amplitudes are denoted $P$ and $S$, respectively, and the complete decay amplitude is

$$\mathcal{A} = S + P\boldsymbol{\sigma} \cdot \hat{\mathbf{n}} \,, \tag{1}$$

where $\hat{\mathbf{n}} = \mathbf{q}/|\mathbf{q}|$ is the direction of the $b$-baryon momentum $\mathbf{q}$ in the $B$-baryon rest frame. The $S$ and $P$ amplitudes are Lorentz scalars and in the two-body decay they have fixed complex-number

| | $\mathcal{B}$ | $\langle\alpha\rangle$ | $\langle\phi\rangle$ | $A_{\rm CP}$ | Comment |
|---|---|---|---|---|---|
| $\Lambda \to p\pi^-$ | 64% | 0.642(13)* | −0.113(61)* | 0.006(21) | PDG18 [7] |
| | | **0.754(3)(2)** | – | **−0.006(12)(7)** | BESIII [8] |
| | | 0.721(6)(5)* | – | – | CLAS [9] |
| | | **0.760(6)(3)** | – | **−0.004(12)(9)** | BESIII [10] |
| $\Lambda \to n\pi^0$ | 36% | 0.65(4)* | – | – | PDG18 [7] |
| | | **−0.692(17)**** | – | – | BESIII [8] |
| $\Sigma^+ \to p\pi^0$ | 52% | −0.980(23)* | 0.628(59)* | – | PDG18 [7] |
| | | **−0.994(4)(2)** | – | **−0.004(37)(1)** | BESIII [11] |
| $\Sigma^+ \to n\pi^+$ | 48% | 0.068(13)* | 2.91(35)* | – | PDG18 [7] |
| $\Sigma^- \to n\pi^-$ | 100% | −0.068(8)* | 0.174(26)* | – | PDG18 [7] |
| $\Xi^0 \to \Lambda\pi^0$ | 100% | −0.406(13)* | 0.36(21)* | – | PDG18 [7] |
| $\Xi^- \to \Lambda\pi^-$ | 100% | −0.458(12)*,° | −0.042(16)* | – | PDG18 [7] [12] |
| | | **−0.373(5)(2)** | **0.016(14)(7)** | **0.006(13)(6)** | BESIII [10] |
| $\Omega^- \to \Lambda K^-$ | 68% | 0.0181(22)* | – | −0.02(13) | PDG18 [7] |
| | | **−0.04(3)** | **1.08(51)** | – | BESIII [13] |

* – result only available for hyperons

** – result only available for antihyperons

° – measured as a product with $\alpha_\Lambda$ value

**Table 1: Properties of two-body hadronic decays of the ground-state hyperons.** The recent BESIII results, in bold, are compared to the world averages before 2018 (reported in PDG18 [7]). In addition BESIII [10] measured $B_{\rm CP} = 0.005(14)(3)$ for $\Xi^- \to \Lambda\pi^-$. Branching fractions $\mathcal{B}$ of the decays are rounded with ±0.5% accuracy.

values. Each of the $L = S, P$ amplitudes can be decomposed in the isospin bases. Using notation from Ref. [15], where $L_{2\Delta I,2I}$ represents a weak transition to the state with isospin $I$ that changes isospin by $|\Delta I|$, the amplitudes for $\Lambda \to p\pi^-$ are

$$L_\Lambda = -\sqrt{\frac{2}{3}} L_{1,1} \exp(i\xi^L_{1,1} + i\delta^L_1) + \sqrt{\frac{1}{3}} L_{3,3} \exp(i\xi^L_{3,3} + i\delta^L_3) \tag{2}$$

and for $\Xi^- \to \Lambda\pi^-$ are

$$L_\Xi = L_{1,2} \exp(i\xi^L_{1,2} + i\delta^L_2) + \frac{1}{2} L_{3,2} \exp(i\xi^L_{3,2} + i\delta^L_2)\ . \tag{3}$$

The contribution of the $|\Delta I| = 3/2$ amplitudes is suppressed and in most studies it is sufficient to consider the $|\Delta I| = 1/2$ transition approximation, where the $S$ and $P$ amplitudes are expressed as

$$S = S_1 \exp(i\xi_S + i\delta_S) \text{ and } P = P_1 \exp(i\xi_P + i\delta_P)\ , \tag{4}$$

with $\xi_S(\xi_P)$ the weak CP-odd phase for the $|\Delta I| = 1/2$ transition and $\delta_S(\delta_P)$ the strong $S(P)$-wave baryon–meson phase-shift at the c.m. energy corresponding to the hyperon mass. For $\Lambda$ decays the $\delta_S(\delta_P)$ phase shifts correspond to the $N$–$\pi$ scattering in the isospin $I = 1/2$ state. The overall

normalisation of the amplitudes, $|S|^2 + |P|^2$, is directly related to the partial decay width

$$\Gamma = \frac{|\mathbf{q}|}{4\pi M_B}(E_b + M_b)(|S|^2 + |P|^2) \,, \tag{5}$$

where $E_b = \sqrt{|\mathbf{q}|^2 + M_b^2}$ and $M_B$, $M_b$ are the baryon masses. The amplitudes can be parameterized using two experimentally motivated decay parameters [16]:

$$\alpha_D := \frac{2\,\mathrm{Re}(S^*P)}{|S|^2 + |P|^2} \;\text{ and }\; \phi_D := \arg\left\{|S-P|^2 - 2|P|^2 + 2S^*P\right\} \,. \tag{6}$$

The parameter $\alpha_D$, $-1 \le \alpha_D \le 1$, for decay $D(B \to b\pi)$ can be determined from the angular distribution asymmetry of the baryon $b$ in the $B$-baryon rest frame. The distribution is given as

$$\frac{1}{\Gamma}\frac{\mathrm{d}\Gamma}{\mathrm{d}\Omega} = \frac{1}{4\pi}\left(1 + \alpha_D \mathbf{P}_B \cdot \hat{\mathbf{n}}\right) \,, \tag{7}$$

where $\mathbf{P}_B$ is the $B$-baryon polarization vector. The parameter $\phi_D$, $-\pi < \phi_D \le \pi$, is related to the rotation of the spin vector between $B$ and $b$ baryons. In a reference system with the $\hat{\mathbf{z}}$-axis along the $b$ momentum in the $B$-baryon rest frame and the $\hat{\mathbf{y}}$ axis along $\mathbf{P}_B \times \hat{\mathbf{z}}$, the $b$-baryon polarization vector is given by [16]

$$\mathbf{P}_b \cdot \hat{\mathbf{z}} = \frac{\alpha_D + \mathbf{P}_B \cdot \hat{\mathbf{z}}}{1 + \alpha_D \mathbf{P}_B \cdot \hat{\mathbf{z}}} \,; \quad \mathbf{P}_b \times \hat{\mathbf{z}} = |\mathbf{P}_B|\sqrt{1-\alpha_D^2}\,\frac{\sin\phi_D\hat{\mathbf{x}} + \cos\phi_D\hat{\mathbf{y}}}{1 + \alpha_D \mathbf{P}_B \cdot \hat{\mathbf{z}}} \,. \tag{8}$$

This means that the transverse component of the $b$-baryon polarization vector is rotated by the angle $\phi_D$ with respect to the $B$-baryon polarization vector (the polarization vectors are defined in the respective baryon rest frame). For $\Xi^- \to \Lambda\pi^-$ with polarized cascade the $\phi_D$ parameter can be determined using the subsequent $\Lambda \to p\pi^-$ decay which acts as a polarimeter. In the phenomenological description of the decays a natural choice of the two independent parameters is $\alpha$ and $\beta$:

$$\alpha := \frac{2\,\mathrm{Re}(S^*P)}{|S|^2 + |P|^2} \;\text{ and }\; \beta := \frac{2\,\mathrm{Im}(S^*P)}{|S|^2 + |P|^2} \,, \tag{9}$$

since they give the real and imaginary part of the interference term between the amplitudes. The $\beta$ and $\phi$ parameters are related as $\beta = \sqrt{1-\alpha^2}\sin\phi$. The branching fractions ($\mathcal{B}$) and the values of the $\alpha$ and $\phi$ parameters for decays of the ground-state octet baryons are listed in Table 1. The amplitudes $\overline{S}$ and $\overline{P}$ for the charge-conjugated (c.c.) decay mode of the antibaryon $\overline{D}(\overline{B} \to \overline{b}\overline{\pi})$ are:

$$\overline{S} = -S_1 \exp(-i\xi_S + i\delta_S) \quad \overline{P} = \;\; P_1 \exp(-i\xi_P + i\delta_P) \,, \tag{10}$$

In the CP-conserving limit the decay parameters $\alpha$, $\beta$ and $\phi$ have the opposite values: $\overline{\alpha} = -\alpha$, $\overline{\phi} = -\phi$ and $\overline{\beta} = -\beta$. Table 1 reports, when available, the hyperon–antihyperon average values defined as

$$\langle\alpha\rangle := \frac{\alpha - \overline{\alpha}}{2}, \quad \langle\phi\rangle := \frac{\phi - \overline{\phi}}{2} \,. \tag{11}$$

The decays can be described using *decay matrices* $a^D_{\mu\nu}$ representing the transformations of the spin operators (Pauli matrices) $\sigma^B_\mu$ and $\sigma^b_\nu$ defined in the $B$ and $b$ baryon rest frames, respectively [17]:

$$\sigma^B_\mu \to \sum_{\nu=0}^{3} a^D_{\mu,\nu}\sigma^b_\nu. \tag{12}$$

The elements of such 4×4 matrices are expressed by the decay parameters $\alpha_D$ and $\phi_D$ and the helicity angles. The matrices are implementations of the Lee–Yang polarization vector transformation Eq. (8) to the specific reference frames used in our approach. The helicity reference frame for baryon $b$ is defined in the following way. In the $B$ rest frame with the $z$ axis defined by the unit vector $\hat{\mathbf{z}}_B$, the direction of the $b$ momentum is denoted as $\hat{\mathbf{p}}_b$. The $b$-baryon helicity system is the $b$ rest frame where the orientation the Cartesian coordinate system is given by the vectors:

$$\hat{\mathbf{x}}_b = \frac{\hat{\mathbf{z}}_B \times \hat{\mathbf{p}}_b}{|\hat{\mathbf{z}}_B \times \hat{\mathbf{p}}_b|} \times \hat{\mathbf{p}}_b, \;\; \hat{\mathbf{y}}_b = \frac{\hat{\mathbf{z}}_B \times \hat{\mathbf{p}}_b}{|\hat{\mathbf{z}}_B \times \hat{\mathbf{p}}_b|} \;\text{ and }\; \hat{\mathbf{z}}_b = \hat{\mathbf{p}}_b \; . \tag{13}$$

In the weak decay $\Omega(\Omega^- \to \Lambda K^-)$ the parity-odd transition is to $d$-wave instead of $s$-wave. Description of a spin-3/2 baryon decay to a spin-1/2 baryon and a pseudoscalar meson is analogous to the decays of spin-1/2 baryons [17]

$$Q_\mu^{\Omega^-} \to \sum_{\nu=0}^{15} b^{\Omega}_{\mu,\nu} \sigma^{\Lambda}_{\nu} \; , \tag{14}$$

where the spin state of the spin-3/2 baryon is described by 16 $Q_\mu$ $\mu = 0, .., 15$ operators. The decay is represented using $16\times4$ decay matrix $b^D_{\mu,\nu}$ with the elements depending on two decay parameters $\alpha_\Omega$ and $\phi_\Omega$.

## 3. Direct CP-violation in kaon and hyperon decays

The conclusive experimental evidence of the direct CP violation in $|\Delta S| = 1$ transitions in kaon two-body hadronic decays was established in 2002 [18, 19]. The effect is quantified by the non-vanishing value of the $\epsilon'/\epsilon$ parameter ratio given by the decay amplitudes of $K_L$ and $K_S$ mesons into pion pairs

$$\frac{\mathcal{A}(K_L \to \pi^+\pi^-)}{\mathcal{A}(K_S \to \pi^+\pi^-)} := \epsilon + \epsilon' \;\text{ and }\; \frac{\mathcal{A}(K_L \to \pi^0\pi^0)}{\mathcal{A}(K_S \to \pi^0\pi^0)} := \epsilon - 2\epsilon' \; . \tag{15}$$

The experimental result $\mathrm{Re}(\epsilon'/\epsilon) = (16.6 \pm 2.3) \cdot 10^{-4}$ [18–20] definitely rules out the superweak CP-violation scenario proposed by Wolfenstein [21] and is consistent with the standard model (SM) prediction via Cabibbo–Kobayashi–Maskawa (CKM) mixing matrix. The CP-violation mechanism in SM requires loop diagrams where all three quark families are involved, the so-called penguin diagrams like the one shown in Fig. 1(a-b). The predictions for $\epsilon'/\epsilon$ had been a challenge for long time due to the partially cancelling contributions from the two types of the penguin diagrams, see e.g. Ref. [22] and references therein. Recently a satisfactory understanding was reached using Lattice [23, 24], $\mathrm{Re}(\epsilon'/\epsilon) = 21.7(82) \times 10^{-4}$, and effective field theory [25–27], $\mathrm{Re}(\epsilon'/\epsilon) = 14(5) \times 10^{-4}$, approaches to Quantum Chromodynamics (QCD). Such progress makes the $\epsilon'/\epsilon$ value one of the important constraints for beyond-SM (BSM) physics scenarios.

The observable CP-violation effect is due to interference between at least two amplitudes with different values of CP-odd and CP-even phases. For the kaon decays the two-pion system can have isospin $I = 0$ and $I = 2$, corresponding to the $|\Delta I| = 1/2$ and $|\Delta I| = 3/2$ transitions, respectively.

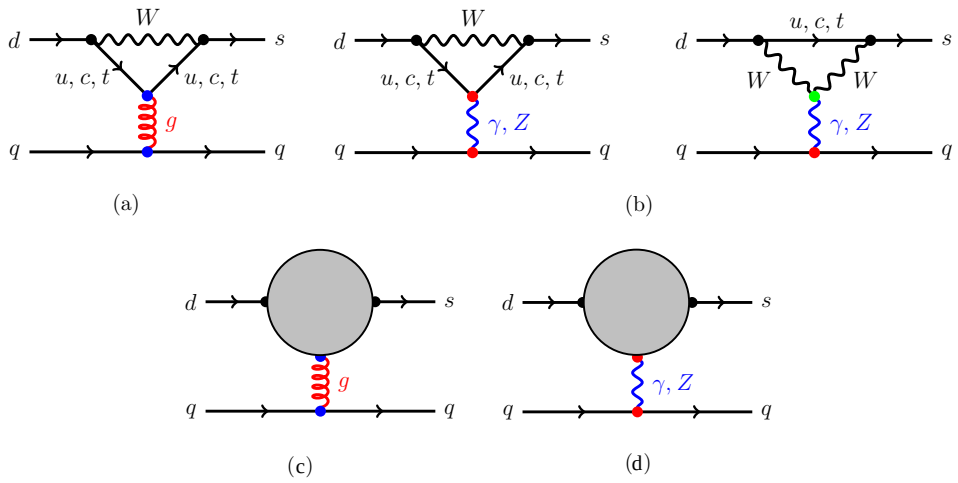


**Figure 1: Quark operators that can generate CP-odd phases in kaon and hyperon decays.** CP-violation effects in kaon decays in SM are given by the (a) QCD-penguin and (b) electroweak-penguin operators. Two types of four-quark operators for BSM scenarios (grey blobs) are given in panels (c) and (d). The hypeon decays are sensitive to the (c) type contributions while kaons probe both. Figure created using a modified script from Ref. [25].

Using notation $A_{2\Delta I,I}$, the isospin decomposition of the amplitudes, Eq. (7.18) from Ref. [28], is written as

$$\mathcal{A}(K^0 \to \pi^+\pi^-) = \sqrt{\frac{1}{3}}A_{3,2}\exp(i\xi_{3,2}+i\delta_2)+\sqrt{\frac{2}{3}}A_{1,0}\exp(i\xi_{1,0}+i\delta_0)$$
$$\mathcal{A}(K^0 \to \pi^0\pi^0) = \sqrt{\frac{2}{3}}A_{3,2}\exp(i\xi_{3,2}+i\delta_2)-\sqrt{\frac{2}{3}}A_{1,0}\exp(i\xi_{1,0}+i\delta_0)\ ,$$

where $\xi_{1,0}$ and $\xi_{3,4}$ are the weak phases corresponding to the $|\Delta I| = 1/2$ and $|\Delta I| = 3/2$ transitions, respectively. The strong phase shifts in the final two-pion systems with isospin $I = 0$ and $I = 2$ are $\delta_0$ and $\delta_2$, respectively. The direct CP-violation, $\epsilon' \neq 0$, requires that the amplitudes $A_{1,0}$ and $A_{3,2}$ must be nonzero. With the above notation $\epsilon'$ is expressed as, Eq. (7.34) from Ref. [28],

$$\epsilon' \backsimeq -\frac{i}{\sqrt{2}}\exp\left(i\delta_2 - i\delta_0\right)\frac{A_{3,2}}{A_{1,0}}(\xi_{1,0}-\xi_{3,2})\ . \tag{16}$$

The direct $|\Delta S| = 1$ CP violation in the two-body hyperon decays, where the spin degrees of freedom generate the two necessary amplitudes, does not require the $|\Delta I| = 3/2$ transitions [29]. Experimentally, there are two independent CP-violation tests that are based on comparison of the decay parameters in $D(B \to b\pi)$ and the c.c. $\overline{D}(\overline{B} \to \overline{b}\overline{\pi})$ processes [30]

$$A_{\rm CP}^D := \frac{\alpha_D + \overline{\alpha}_D}{\alpha_D - \overline{\alpha}_D}, \quad \Phi_{\rm CP}^D := \frac{\phi_D + \overline{\phi}_D}{2}\ . \tag{17}$$

Using Eqs. (4) and (10) they can be expressed as

$$A_{\rm CP} = -\frac{\sqrt{1-\alpha^2}}{\alpha}\sin\phi\tan(\xi_P-\xi_S) = -\frac{\beta}{\alpha}\tan(\xi_P-\xi_S) \tag{18}$$

$$= -\tan(\delta_P-\delta_S)\tan(\xi_P-\xi_S) \tag{19}$$

$$\Phi_{\rm CP} = \frac{\alpha}{\sqrt{1-\alpha^2}}\cos\phi\tan(\xi_P-\xi_S) \tag{20}$$

$$B_{\rm CP} := \frac{\beta+\overline{\beta}}{\alpha-\overline{\alpha}} = \tan(\xi_P-\xi_S)\,, \tag{21}$$

where an additional $B_{\rm CP}$ observable, related to the $\beta$ parameters comparison, was introduced. As one can see all three CP-violation observables are related and provide a measure of the single quantity $\tan(\xi_P-\xi_S)$ — the weak-phase difference.

| | $\xi_P-\xi_S$ | | | $C_B$ | $C'_B$ |
|---|---|---|---|---|---|
| | $(\eta\lambda^5A^2)$ | $[10^{-4}$ rad] | $[10^{-2}$ rad] | | |
| | SM Ref. [31] | | Exp | BSM Ref. [32] | |
| $\Lambda\to p\pi^-$ | $0.2\pm1.6$ | $0.3\pm2.2$ | $4.7\pm9.4$ | $1.1\pm2.2$ | $0.4\pm0.8$ |
| $\Xi^-\to\Lambda\pi^-$ | $-1.4\pm1.2$ | $-1.9\pm1.6$ | $1.2\pm3.5$ | $-0.5\pm1.0$ | $0.4\pm0.7$ |

**Table 2: Weak-phase difference in hyperon decays.** (left) Standard Model predictions [31] compared to the BESIII measurements. (right) Parameters $C_B$ and $C'_B$ used in Eq. (34) to relate the weak-phase differences in hyperon decays to the BSM constraints from the kaon observables [32].

Two hyperon decays are considered to be sensitive probes of the CP-violation: (1) $\Lambda(\Lambda\to p\pi^-)$ and (2) $\Xi(\Xi^-\to\Lambda\pi^-)$. The decay (2) is studied using the $\Lambda$ decay mode (1) as the subsequent process. In the following the decay parameters related to the decay (1) and (2) will be denoted by the $\Lambda$ and $\Xi$ indices, respectively. The SM contribution to $\xi_P$ and $\xi_S$ for $\Lambda\to p\pi^-$ and $\Xi^-\to\Lambda\pi^-$ via the CKM mechanism is $O(10^{-5})$ and $O(10^{-4})$, respectively, as it can be read from the predictions [31] given in Table 2. The value of the product of the Wolfenstein parameters $\eta\lambda^5A^2$ is $1.37\times10^{-4}$ according to the latest PDG report [33]. The difference between the values for the two decays is due to the opposite signs of the $\xi_P$ phases in the predictions. The relation between $\xi_P-\xi_S$ values and the kaon observables $\epsilon$ and $\epsilon'$ is discussed in Sec. 6.

A dedicated experiment HyperCP (E871) at Fermilab [34] running 1996–99 has set the world's best limits on the CP violation in the $\Xi^-\to\Lambda\pi\to p\pi^-\pi^-$ decay sequence. A secondary cascade beam was produced by 800 GeV primary protons interacting with a copper target. The beam was momentum and charge-sign selected. The sum of the asymmetries $A^{\Xi}_{\rm CP}+A^{\Lambda}_{\rm CP} = 0(5)(4)\times10^{-4}$ [35] was determined using data sample of $117\times10^6$ $\Xi^-$ and $41\times10^6$ $\overline{\Xi}^+$ with unpolarized beams. A preliminary result of $A^{\Xi}_{\rm CP}+A^{\Lambda}_{\rm CP} = -6(2)(2)\times10^{-4}$ based on the full data sample of $862\times10^6$ $\Xi$ and $230\times10^6$ $\overline{\Xi}$ was presented at the BEACH2008 conference [36]. Since no final result was published one can suspect an inherent problem to understand the systematic effects at the level of $4\times10^{-4}$. The most precise $\phi_\Xi$ value contributing to the PDG18 average reported in Table 1 was measured using $144\times10^6$ $\Xi^-$ events with average polarization of $\sim 5\%$ [12]. The drawback of the HyperCP experimental method is the non-charge-conjugation-symmetric production mechanism and the need to use separate runs with different settings for the baryon and antibaryon measurements.

| | Final state | $\mathcal{B}(\times 10^{-4})$ | $\alpha_\psi$ | $\Delta\Phi$(rad) | References |
|---|---|---|---|---|---|
| $J/\psi \to$ | $\Lambda\ \overline{\Lambda}$ | 19.43(3) | 0.461(9) | 0.740(13) | [8, 37] |
| | $\Sigma^+\ \overline{\Sigma}^-$ | 15.0(24) | −0.508(7) | −0.270(15) | [11, 38] |
| | $\Sigma^-\ \overline{\Sigma}^+$ | | — no data — | | |
| | $\Sigma^0\ \overline{\Sigma}^0$ | 11.64(4) | −0.449(20) | – | [37] |
| | $\Xi^0\ \overline{\Xi}^0$ | 11.65(43) | 0.66(6) | – | [39] |
| | $\Xi^-\ \overline{\Xi}^+$ | 9.7(8) | 0.586(16) | 1.213(48) | [10, 33] |
| $\psi' \to$ | $\Sigma^+\ \overline{\Sigma}^-$ | 2.32(12) | 0.682(11) | 0.379(16) | [11] |

**Table 3: Properties of some of the $e^+e^- \to J/\psi, \psi' \to B\overline{B}$ hyperon–antihyperon production reactions** involving the ground-state octet baryons.

In addition the accuracy of the $\phi_\Xi$ parameter determination is limited by the low value of the $\Xi^-$-beam polarization. In the next section a novel method for the hyperon CP-violation studies is described.

## 4. Production of baryon–antibaryon pairs and joint angular distributions

The $e^+e^- \to J/\psi, \psi' \to B\overline{B}$ processes listed in Table 3 have relatively large branching fractions and can be used for determination of hyperon decay properties and CP-violation tests. Two analysis methods are possible: (1) exclusive (double tag, DT) where the decay chains of the baryon and antibaryon are fully reconstructed and (2) inclusive (single tag, ST) where only the decay chain of the baryon or antibaryon is reconstructed but the two-body production process is identified and its kinematics fully determined using missing energy/mass technique.

To describe a baryon–antibaryon pair production in electron–positron annihilation including the two-body sequential hyperon decays a modular approach developed in Ref. [17] can be used. The spin-density matrices defined in helicity reference frames keep track of the spin information in the hyperon decay chains. The base vectors of the helicity reference frames are uniquely defined by the recursion of Eq. (13). The $z$-axis in the electron–positron annihilation c.m. system is taken to be the positron-momentum direction. The joint spin-density matrix of the $B\overline{B}$ pair is:

$$\rho_{B\overline{B}} = \sum_{\mu,\nu=0}^{3} C_{\mu\nu}\, \sigma_\mu^B \otimes \sigma_\nu^{\overline{B}}\,, \tag{22}$$

where $\sigma_\mu^B(\sigma_\nu^{\overline{B}})$ is the set of Pauli matrices in the $B(\overline{B})$-baryon helicity frame and $C_{\mu\nu}$ is $4\times 4$ real-number matrix representing polarizations and spin correlations. It describes the spin configuration of the entangled hyperon–antihyperon pair in their respective helicity frames. As a consequence of the base-vectors definition in Eq. (13) the relative orientation of the axes in the helicity frames for $B$ $(\hat{\mathbf{x}}_1, \hat{\mathbf{y}}_1, \hat{\mathbf{z}}_1)$ and for $\overline{B}$ $(\hat{\mathbf{x}}_2, \hat{\mathbf{y}}_2, \hat{\mathbf{z}}_2)$ is $(\hat{\mathbf{x}}_2, \hat{\mathbf{y}}_2, \hat{\mathbf{z}}_2) = (\hat{\mathbf{x}}_1, -\hat{\mathbf{y}}_1, -\hat{\mathbf{z}}_1)$. The coefficients $C_{\mu\nu}^{1/2}$ depend on the angle $\theta$ between the positron and baryon $B$. The final state baryons can have $\pm 1/2$ helicities but due to the parity conservation only two transitions are independent: $h_1 := A_{1/2,1/2} = A_{-1/2,-1/2}$ and $h_2 := A_{1/2,-1/2} = A_{-1/2,1/2}$. Therefore the $e^+e^- \to B\overline{B}$ process at fixed c.m. energy is described

by two complex form factors. If the overall normalisation is irrelevant two real parameters can be used:

$$\alpha_\psi := \frac{|h_2|^2 - 2|h_1|^2}{|h_2|^2 + 2|h_1|^2};\ -1 \le \alpha_\psi \le 1 \text{ and } \Delta\Phi := \arg(h_1/h_2). \tag{23}$$

The structure of the $C^{1/2}_{\mu\nu}$ matrix can be represented by the polarization vector $P_y = P_y(\theta)$ and spin correlations $C^{1/2}_{ij} = C^{1/2}_{ij}(\theta)$ as

$$C^{1/2}_{\mu\nu} = 3\frac{1+\alpha_\psi\cos^2\theta}{3+\alpha_\psi}\begin{pmatrix} 1 & 0 & P_y & 0 \\ 0 & C_{xx} & 0 & C_{xz} \\ -P_y & 0 & C_{yy} & 0 \\ 0 & -C_{xz} & 0 & C_{zz} \end{pmatrix}. \tag{24}$$

The $C^{1/2}_{\mu\nu}$ matrix is [17]:

$$\frac{3}{3+\alpha_\psi}\begin{pmatrix} 1+\alpha_\psi\cos^2\theta & 0 & \beta_\psi\sin\theta\cos\theta & 0 \\ 0 & \sin^2\theta & 0 & \gamma_\psi\sin\theta\cos\theta \\ -\beta_\psi\sin\theta\cos\theta & 0 & \alpha_\psi\sin^2\theta & 0 \\ 0 & -\gamma_\psi\sin\theta\cos\theta & 0 & -\alpha_\psi-\cos^2\theta \end{pmatrix}, \tag{25}$$

using notation $\beta_\psi = \sqrt{1-\alpha_\psi^2}\sin(\Delta\Phi)$ and $\gamma_\psi = \sqrt{1-\alpha_\psi^2}\cos(\Delta\Phi)$. The $B$-baryon angular distribution is

$$\frac{1}{\sigma}\frac{\mathrm{d}\sigma}{\mathrm{d}\Omega_B} = \frac{3}{4\pi}\frac{1+\alpha_\psi\cos^2\theta}{3+\alpha_\psi}. \tag{26}$$

The complete double-tagged joint angular distribution of the $e^+e^- \to B\overline{B}$ process with a single step decay $D(B \to b\pi)$ + c.c. is

$$\mathcal{W}(\boldsymbol{\xi};\boldsymbol{\omega}) = \sum_{\mu,\nu=0}^{3} C^{1/2}_{\mu\nu} a^D_{\mu 0} a^{\overline{D}}_{\nu 0}, \tag{27}$$

where the vector $\boldsymbol{\xi}$ denotes the complete set of the spherical coordinates in the helicity frames (*helicity angles*) describing the event. The global parameter vector $\boldsymbol{\omega}$ has four dimensions: $\boldsymbol{\omega} := (\alpha_\psi, \Delta\Phi, \alpha_D, \overline{\alpha}_D)$. Of importance for the joint angular distribution for a single-step weak decay like $\Lambda \to p\pi^-$ is that $\Delta\Phi \neq 0$ and the $\Lambda$ and $\overline{\Lambda}$ are produced with a transverse polarization. Only the polarization and spin correlations allow for a simultaneous and independent determination of $\alpha_\Lambda$ and $\overline{\alpha}_\Lambda$, using the method proposed in Ref. [6].

The production and the two-step decays in the $e^+e^- \to \Xi^-\overline{\Xi}^+$ are described by a nine dimensional vector $\boldsymbol{\xi}$ of the helicity angles. The structure of the nine-dimensional angular distribution is determined by eight global parameters $\boldsymbol{\omega}_\Xi := (\alpha_\psi, \Delta\Phi, \alpha_\Xi, \phi_\Xi, \overline{\alpha}_\Xi, \overline{\phi}_\Xi, \alpha_\Lambda, \overline{\alpha}_\Lambda)$ and in the modular form give as [17]:

$$\mathcal{W}(\boldsymbol{\xi};\boldsymbol{\omega}_\Xi) = \sum_{\mu,\nu=0}^{3} C^{1/2}_{\mu\nu} \sum_{\mu'\nu'=0}^{3} a^{\Xi}_{\mu\mu'} a^{\overline{\Xi}}_{\nu\nu'} a^{\Lambda}_{\mu' 0} a^{\overline{\Lambda}}_{\nu' 0}. \tag{28}$$

The general expression for the joint density matrix for the spin-3/2 $B\overline{B}$ pair is [17]:

$$\rho_{B\overline{B}} = \sum_{\mu,\nu=0}^{15} C^{3/2}_{\mu\nu}\, Q^B_\mu \otimes Q^{\overline{B}}_\nu, \tag{29}$$

where a set of 16 base matrices $Q^B_\mu(Q^{\overline{B}}_\nu)$ in the $B(\overline{B})$ rest frame is used and $C^{3/2}_{\mu\nu}$ is 16×16 real matrix representing polarizations and spin correlations. The complete joint distribution of $e^+e^- \to \Omega^-\overline{\Omega}^+$ with subsequent decays $\Omega(\Omega^- \to \Lambda K^-)$, $\Lambda(\Lambda \to p\pi^-)$ + c.c. in the nine dimensional phase space of the vector $\boldsymbol{\xi}$ of kinematic variables is given by the modular expression with similar structure as Eq. (28)

$$\mathcal{W}(\boldsymbol{\xi};\boldsymbol{\omega}_\Omega) = \sum_{\mu,\nu=0}^{15} C^{3/2}_{\mu\nu} \sum_{\mu'\nu'=0}^{3} b^{\Omega}_{\mu\mu'} b^{\overline{\Omega}}_{\nu\nu'} a^{\Lambda}_{\mu'0} a^{\overline{\Lambda}}_{\nu'0} \,. \tag{30}$$

However, the spin-correlations–polarization matrix $C^{3/2}_{\mu\nu}$ depends on four complex form factors $\mathbf{h}_k$, $k = 1,2,3,4$. They can be parameterized by six real numbers where $\mathbf{h}_k = h_k \exp i\phi_k$ with $h_k = |\mathbf{h}_k|$, $h_2 = 1$ (overall normalisation) and $\phi_2 = 0$ (overall phase) as in the BESIII analysis. The elements of the $16 \times 4$ $b^{\Omega}_{\mu\mu'}$ matrices describing $\Omega$ decay to $\Lambda$ and $K^-$ depend on the two decay parameters: $\alpha_\Omega$ and $\phi_\Omega$. The angular distribution in a single-tag experiment is

$$\mathcal{W}(\boldsymbol{\xi};\boldsymbol{\omega}_\Omega) = \sum_{\mu=0}^{15} C^{3/2}_{\mu 0} \sum_{\mu'=0}^{3} b^{\Omega}_{\mu\mu'} a^{\Lambda}_{\mu'0} := \sum_{\mu=0}^{15} r_\mu \sum_{\mu'=0}^{3} b^{\Omega}_{\mu\mu'} a^{\Lambda}_{\mu'0} \,, \tag{31}$$

where the polarization terms $C^{3/2}_{\mu 0}$ are denoted as $r_\mu$ in the BESIII analysis and only terms $r_0$, $r_1$, $r_6$, $r_7$, $r_8$, $r_{10}$ and $r_{11}$ are nonzero.

### 4.1 Experimental method

The BESIII Collaboration has the world's largest data samples of the $e^+e^- \to J/\psi, \psi \to B\overline{B}$ processes. The so-far-released analyses are based on $1.31 \times 10^9$ $J/\psi$ and $(448.1 \pm 2.9) \times 10^6$ $\psi'$ events but $10^{10}$ $J/\psi$ and $3 \times 10^9$ $\psi'$ events are now collected. The general analysis strategy requires determination for each event consistent with the signal hypothesis the complete set of helicity angles $\boldsymbol{\xi}_i$ from the intermediate and final-state particle momenta. The physical parameters in the $\boldsymbol{\omega}$ vector are then determined by an unbinned maximum log-likelihood (MLL) fit where the multidimensional detection efficiency $\epsilon(\boldsymbol{\xi})$ is taken into account. The likelihood function is

$$\mathcal{L}(\boldsymbol{\xi}_1, \boldsymbol{\xi}_2, ..., \boldsymbol{\xi}_N; \boldsymbol{\omega}) = \prod_{i=1}^{N} \frac{\mathcal{W}(\boldsymbol{\xi}_i;\boldsymbol{\omega})\epsilon(\boldsymbol{\xi}_i)}{\mathcal{N}(\boldsymbol{\omega})} \,, \tag{32}$$

where $N$ is the number of selected events, $\mathcal{W}(\boldsymbol{\xi};\boldsymbol{\omega})$ is the angular distribution specified by one of the Eqs. (27,28,30), and the normalisation factor $\mathcal{N}(\boldsymbol{\omega}) = \int \mathcal{W}(\boldsymbol{\xi};\boldsymbol{\omega})\epsilon(\boldsymbol{\xi})\mathrm{d}\boldsymbol{\xi}$. The normalisation factor is approximated as $\mathcal{N}(\boldsymbol{\omega}) \approx \frac{1}{M}\sum_{j=1}^{M} \mathcal{W}(\boldsymbol{\xi}_j;\boldsymbol{\omega})$, using $M$ Monte Carlo (MC) events generated uniformly over the phase space, propagated through the detector and reconstructed in the same way as data. $M$ is chosen to be significantly larger than the number of events in data. By taking the log-likelihood function, the efficiency function in the nominator is separated as an additive term which only affects the overall normalisation since the detection efficiency is not dependent on the $\boldsymbol{\omega}$ parameter vector.

## 5. The BESIII results

### 5.1 $e^+e^- \to J/\psi \to \Lambda\overline{\Lambda}$

The initial observation of the polarization in $e^+e^- \to J/\psi \to \Lambda\overline{\Lambda}$ at BESIII [8] was reported in 2018. The final data samples have 420,593 and 47,009 events with an estimated background of $399 \pm 20$ and $66 \pm 8$ events for the $p\pi^-\overline{p}\pi^+$ and $p\pi^-\overline{n}\pi^0$ final states, respectively. A clear polarization

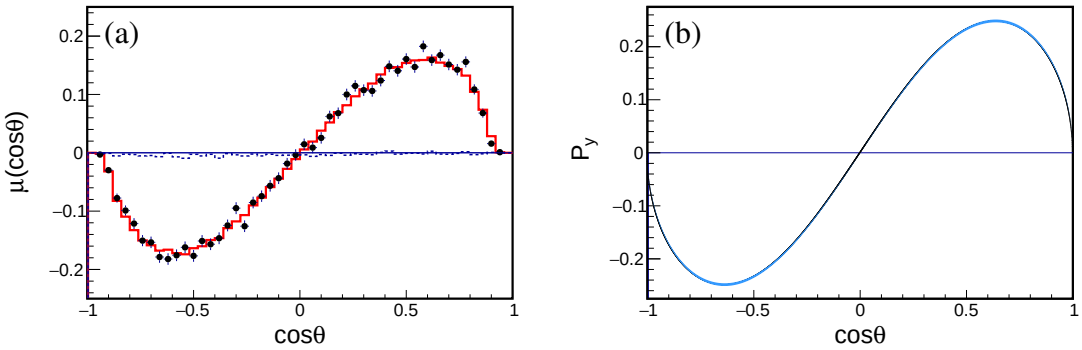


**Figure 2: Spin polarization in $e^+e^- \to J/\psi \to \Lambda\overline{\Lambda}$.** (a) Moment $\mu(\cos\theta)$ using data not corrected for efficiency as a function of $\cos\theta$. The points with error bars are the BESIII data, and the solid-line histogram is the global fit results. The dashed histogram shows the no polarization scenario. (b) Polarization of $\Lambda$ as a function of $\cos\theta$ calculated using the values of $\alpha_\psi$ and $\Delta\Phi$ from the MLL fit.

signal, dependent on the $\Lambda$ direction, $\cos\theta$, is observed for $\Lambda$ and $\overline{\Lambda}$. In Fig. 2(a) the moment

$$\mu(\cos\theta) = \frac{m}{N} \sum_i^{N_k} \left( \hat{\mathbf{n}}_p^{(i)} \cdot \hat{\mathbf{y}}_1 - \hat{\mathbf{n}}_{\overline{p}}^{(i)} \cdot \hat{\mathbf{y}}_2 \right) \tag{33}$$

related to the polarization is calculated for $m = 50$ bins in $\cos\theta$. $N$ is the total number of events in the data sample and $N_k$ is the number of events in $k$-th $\cos\theta$ bin. The expected angular dependence is $\mu(\cos\theta) \sim (\alpha_\Lambda - \overline{\alpha}_\Lambda) \cdot C_{02}$ for the acceptance corrected data. The phase between helicity flip and helicity conserving transitions is determined to be $\Delta\Phi = (42.4 \pm 0.6 \pm 0.5)^\circ$. This value of the phase corresponds to the transverse polarization $P_y$ as shown in Fig. 2(b) reaching maximum of 25%. The nonzero value of $\Delta\Phi$ enables a simultaneous determination of the decay asymmetry parameters for $\Lambda \to p\pi^-$, $\overline{\Lambda} \to \bar{p}\pi^+$, and $\overline{\Lambda} \to \bar{n}\pi^0$ reported in Table 1.

### 5.2 $e^+e^- \to J/\psi, \psi' \to \Sigma^+\overline{\Sigma}^-$

Study of baryon–antibaryon pair production involving isospin-1 baryons such as $\Sigma$ can help to understand the dynamics of the final-state interactions leading to the nonzero $\Delta\Phi$ phase. The process $e^+e^- \to J/\psi, \psi' \to \Sigma^+\overline{\Sigma}^-$ studied using the $\Sigma p(\Sigma^+ \to p\pi^0)$ decay mode is interesting in the context of revealing quantum entangled spin correlations, since the large value of the asymmetry parameter $|\alpha_{\Sigma p}| \approx 1$ makes some of the quantum mechanics tests possible [40]. The PDG18 value of the decay parameter $\alpha_{\Sigma p}$ given in Table 1 was based on the $\pi^+ p \to \Sigma^+ K^+$ experiments fifty years ago [41–43] while $\overline{\alpha}_{\Sigma p}$ has not been measured. In the BESIII measurement [11] data at the $J/\psi$ and $\psi'$ resonances are analysed using the DT technique. The $\alpha_{J/\psi}$ parameter is determined to be

negative and $\alpha_{\psi'}$ positive. The spin polarization of the $\Sigma^+$ baryons is observed for both datasets. The relative phases between the helicity amplitudes in the $J/\psi$ and $\psi'$ decays have opposite signs and the magnitudes given in Table 3. The polarizations are illustrated in Fig. 3, using the acceptance uncorrected moment $\mu(\cos\theta)$. Since $\Delta\Phi$ is nonzero, a simultaneous measurement of $\alpha_{\Sigma p}$ and $\overline{\alpha}_{\Sigma p}$ is performed using both data sets. The average $\langle\alpha_{\Sigma p}\rangle$ is reported in the Table 1. The CP-odd observable $A_{\rm CP}^{\Sigma p} = -0.004 \pm 0.037 \pm 0.010$ is extracted for the first time, however, the SM prediction for the CP violation is $A_{\rm CP}^{\Sigma p} \sim 3.6 \times 10^{-6}$ [31], an order of magnitude lower than for the $\Lambda$ and $\Xi$ decays.

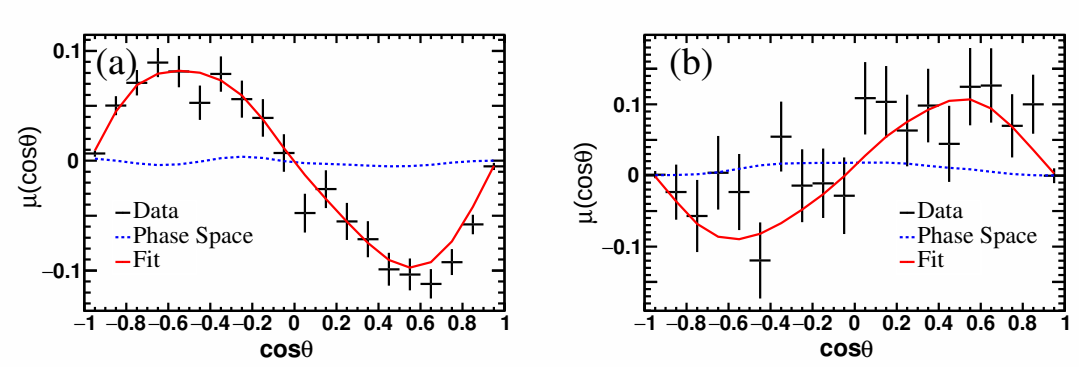


**Figure 3: Spin polarization in $e^+e^- \to J/\psi, \psi' \to \Sigma^+\overline{\Sigma}^-$.** The moments $\mu(\cos\theta)$ using data not corrected for efficiency as function of $\cos\theta$ for the decays $J/\psi \to \Sigma^+\overline{\Sigma}^-$ (a) and $\psi' \to \Sigma^+\overline{\Sigma}^-$ (b). The points with error bars are experimental data, the red lines are the fit results and the blue-dashed lines represent the distributions without polarization.

### 5.3 $e^+e^- \to \psi' \to \Omega^-\overline{\Omega}^+$

Surprisingly the $J = 3/2$ spin value of the $\Omega^-$ baryon was not confirmed experimentally in the model independent way. For example the BaBar analysis [44] assumed the spins of $\Xi_c^0$ and $\Omega_c^0$ of $J = 1/2$ according to the quark model assignment. In the BESIII analysis [13] the process $e^+e^- \to \psi' \to \Omega^-\overline{\Omega}^+$ was studied using the ST method, where the reconstructed decay chain was $\Omega^- \to K^-\Lambda$, $\Lambda \to p\pi^-$. Total 4035 ± 76 $\psi' \to \Omega^-\overline{\Omega}^+$ signal events were reconstructed where only the $\Omega^-$ or $\overline{\Omega}^+$ is reconstructed and the $\overline{\Omega}^+$ or $\Omega^-$ on the recoil side is inferred from the missing mass of the reconstructed particles. Two $\Omega^-$ spin hypotheses, $J = 1/2$ or $J = 3/2$, are tested using the joint angular distribution of the sequential decays of $e^+e^- \to \Omega^-\overline{\Omega}^+$ process. For the $J = 1/2$ hypothesis, two form factors are needed and for $J = 3/2$ hypothesis, the annihilation process involves four complex form factors [45]. In addition to vector polarization, the spin-3/2 fermions can have quadrupole and octupole polarization [1, 46]. Polarization of the $\Omega^-$ can be studied using the chain of weak decays $\Omega^- \to K^-\Lambda$ and $\Lambda \to p\pi^-$, where the first decay is described by the decay parameters $\alpha_\Omega$ and $\phi_\Omega$ between the parity-conserving $P$-wave and parity-violating $D$-wave ($S$-wave for $J = 1/2$ hypothesis) decay amplitudes. A simultaneous fit is performed to the $\Omega^-$ and $\overline{\Omega}^+$ events with the constraint $\phi_\Omega = -\phi_{\overline{\Omega}}$. The likelihood ratio $t$ between the two spin hypotheses is used as a test variable [47]. The MC sample for each hypothesis is generated according to the corresponding joint angular distribution, propagated through the detector model and subjected to the same event selection criteria as the experimental data. The test statistic $t$ distribution is shown in Fig. 4(a). The

two well separated right and left peaks are for the $J = 1/2$ and $J = 3/2$ hypotheses, respectively. The position of the measured $t$-value unambiguously favours the $J = 3/2$ hypothesis.

**Table 4:** Magnitudes and phases of the helicity amplitudes in the $e^+e^- \to \psi' \to \Omega^-\overline{\Omega}^+$ process.

| parameter | solution | alt. solution |
|---|---|---|
| $h_1$ | 0.30±0.11±0.04 | |
| $\phi_1$ | 0.69±0.41±0.13 | 2.38±0.37±0.13 |
| $h_3$ | 0.26±0.05±0.02 | |
| $\phi_3$ | 2.60±0.16±0.08 | |
| $h_4$ | 0.51±0.03±0.01 | |
| $\phi_4$ | 0.34±0.80±0.31 | 1.37±0.68±0.16 |

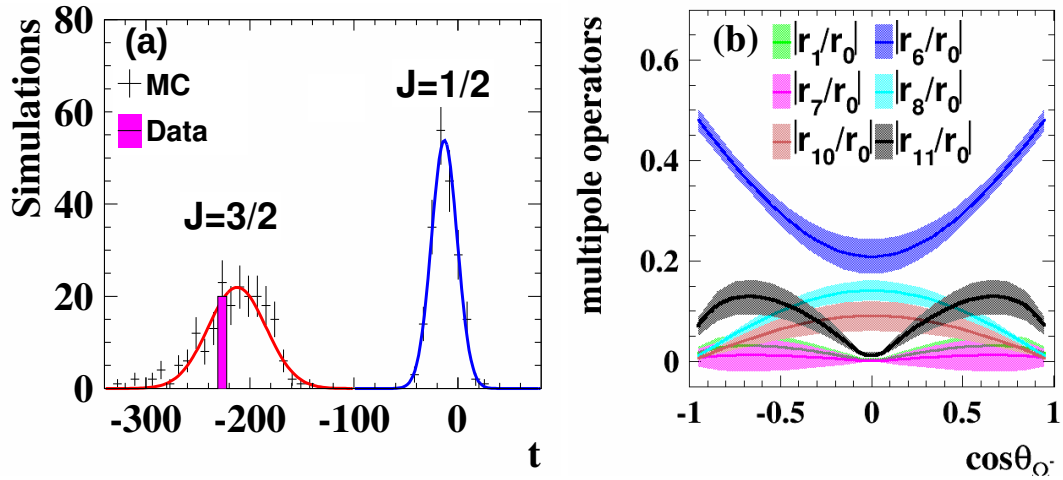


**Figure 4: BESIII results for $e^+e^- \to \psi' \to \Omega^-\overline{\Omega}^+$.** (a) Distribution of the test statistic $t$ for a series of MC experiments under the $J = 1/2$ (right peak) and $J = 3/2$ (left peak) hypotheses. The lines represent Gaussian fits to the simulated data points. The $t$ value obtained from experimental data is indicated by the vertical bar. (b) Angular dependence of the polarization terms $r_i$. The solid lines represent the central values, and the shaded areas represent ±1 standard deviation.

The fit with the $J = 3/2$ hypothesis has two solutions for the helicity amplitudes shown in Table 4. The magnitudes of the amplitudes are the same within errors for the two solutions while the phases $\phi_1$ and $\phi_4$ significantly differ. The amplitude $\mathbf{h}_2 = A_{1/2,-1/2}$ dominates the decay process since $h_2$ is fixed to one and the values of other magnitudes $h_i$ are lower. The parameter $\alpha_\psi$ describing the angular distribution of the $\Omega^-$ determined from the magnitudes $h_i$ is $\alpha_\psi = 0.24 \pm 0.10$. The $\cos\theta$ dependence of the multipolar polarization operators $r_i$ is shown in Fig. 4(b). In the $e^+e^- \to \psi' \to \Omega^-\overline{\Omega}^+$ process the $\Omega^-$ can have vector ($r_1$), quadrupole ($r_6$, $r_7$, $r_8$) and octupole ($r_{10}$, $r_{11}$) polarization components [1, 46].

The value of $\phi_\Omega$ provides information if the transition is $p$-wave dominant ($\phi_\Omega = 0$) or $d$-wave dominant ($\phi_\Omega = \pi$). Contrary to the theoretical predictions of the $P$-wave dominance [48], the $d$-wave dominant solution is preferred,. The ratio of $D$- to $P$-wave transitions $|A_D|^2/|A_P|^2$ is

$2.4 \pm 2.0$ or $3.3 \pm 2.9$, depending on the solution. Allowing $\alpha_\Omega$ to be determined by the fit, one obtains $\alpha_\Omega = -0.04 \pm 0.03$, which is consistent with the previous measurements [49–51].

### 5.4 $e^+e^- \to J/\psi \to \Xi^-\overline{\Xi}^+$ (preliminary) [10]

The recent BESIII analysis [10] of the $J/\psi \to \Xi^-\overline{\Xi}^+$ process uses double-tag method with fully reconstructed $\Xi^-\overline{\Xi}^+ \to \Lambda\pi^-\overline{\Lambda}\pi^+ \to p\pi^-\pi^-\overline{p}\pi^+\pi^+$ events. The $\Lambda(\overline{\Lambda})$ candidates are identified by combining $p\pi^-(\overline{p}\pi^+)$ pairs and the $\Xi^-(\overline{\Xi}^+)$ candidates by subsequently combining $\Lambda\pi^-(\overline{\Lambda}\pi^+)$ pairs. After applying all selection criteria, there are 73,244 $\Xi^-\overline{\Xi}^+$ signal candidates with the remaining background of $187 \pm 16$ events. The weak-decays parameters and the production related parameters $\alpha_\psi$ and $\Delta\Phi$ are determined by the MLL fit to the angular distribution Eq. (28). The results are summarised in Tables 1 and 3. The fit quality is illustrated in Fig. 5 using the acceptance corrected diagonal spin correlations and polarization defined in Eq. (24). The data points are determined by independent fits for each of the $\cos\theta$ ranges, without assumptions on the $\cos\theta$ dependence of $C_{\mu\nu}$. The red curves represent the angular dependence obtained with the parameters $\alpha_\psi$ and $\Delta\Phi$ determined from the global MLL fit. The independently determined data points agree well with the globally fitted curves.

Both decay parameters for the $\Xi(\Xi^- \to \Lambda\pi^-)$ decay as well as the $\alpha_\Lambda$ parameter for $\Lambda(\Lambda \to p\pi^-)$ and for the c.c. processes are determined. The multi-step process enhances the angular correlations between the baryons and antibaryons to such an extent that $\alpha_\Xi$ and $\alpha_\Lambda$ the polarization of the $\Xi^-\overline{\Xi}^+$ pair plays a minor role [52]. The comparison of the determined decay parameters for baryons and antibaryons allows for three independent CP symmetry tests reported in Table. 1. The asymmetries $A_{\rm CP}^\Xi$ and $\Phi_{\rm CP}^\Xi$ are measured for the first time.

The BESIII result for $\langle\phi_\Xi\rangle$ has similar precision as HyperCP result for $\phi_\Xi = -0.042(16)$ [12] but the two values differ by 2.6 standard deviations. The measurement of $\langle\phi_\Xi\rangle$ translates to the determination of the strong phase difference $(\delta_P - \delta_S)$ of $(-4.0 \pm 3.3 \pm 1.7) \times 10^{-2}$ consistent with the heavy-baryon chiral perturbation theory predictions of $(1.9 \pm 4.9) \times 10^{-2}$ [31]. The weak phase difference $(\xi_P - \xi_S)$ (equivalent to the $B_{\rm CP}^\Xi$ observable) is extracted by applying Eq. (20) and compared to the SM predictions in Table. 2. This is one of the most precise tests of the CP symmetry for strange baryons and the first direct measurement of the weak phase for any baryon.

## 6. Discussion

### 6.1 Status of the $\alpha_\Lambda$ decay parameter

The $\alpha_\Lambda$ parameter plays an important role in the analyses involving polarization of $\Lambda$ hyperon. The BESIII result on $\langle\alpha_\Lambda\rangle$ of 0.754(3)(2) [8] deviating by 17% from the world average for the $\alpha_\Lambda$ parameter of 0.642(13) [7] established forty years ago calls for verification by independent measurements. The BESIII result has gained support from a re-analysis of CLAS data on $\gamma p \to \Lambda K^+$ [9]. The CLAS result for $\alpha_\Lambda$ of 0.721(6)(5) is in better agreement with BESIII than with the PDG18 value, but there is a discrepancy that needs to be understood. Sequential $\Xi^-$ decays provide an independent measurement of the $\Lambda$ decay parameters $\alpha_\Lambda$ and $\alpha_{\overline{\Lambda}}$. The measured value of $\langle\alpha_\Lambda\rangle$ is in excellent agreement with that obtained from the $J/\psi \to \Lambda\overline{\Lambda}$ analysis. Figure 6 compares the latest measurements as the ideograms representing the combined statistical and systematic uncertainties.

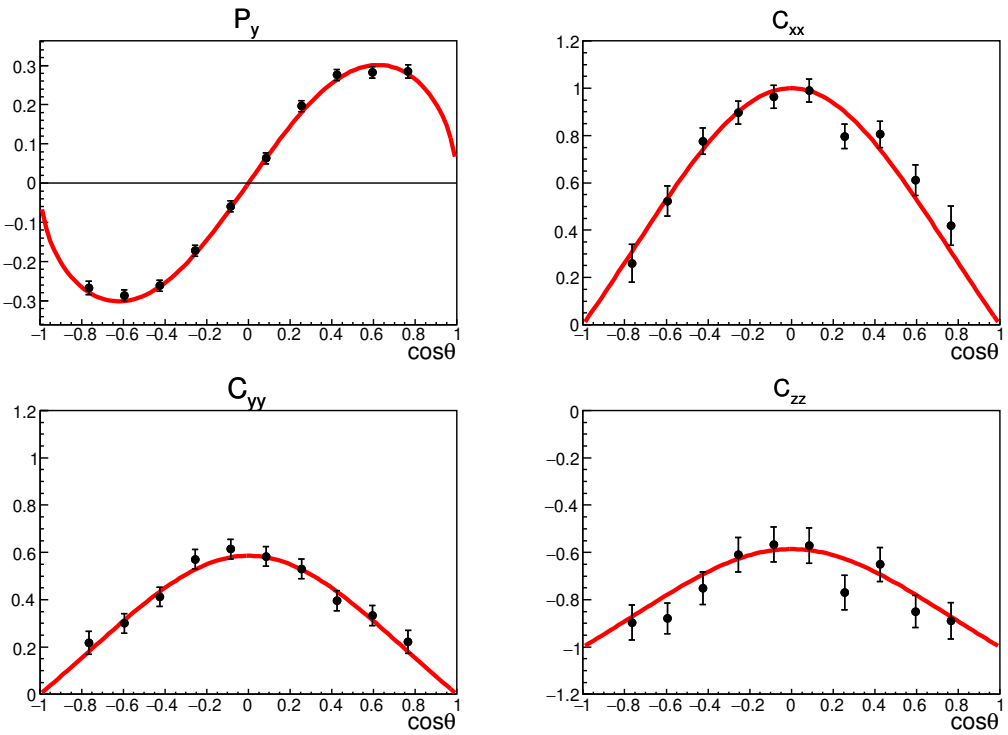


**Figure 5: (Prel. results) Polarization and spin correlations and in the $e^+e^- \to \Xi^-\bar{\Xi}^+$ reaction** (a) $P_y$, (b) $C_{xx}$, (c) $C_{yy}$ and (d) $C_{zz}$ as functions of $\cos\theta$. The data points are determined independently in each bin. The red curves represent the expected angular dependence obtained with the values of $\alpha_\psi$ and $\Delta\Phi$ from the global fit. The errors bars indicate the statistical uncertainties.

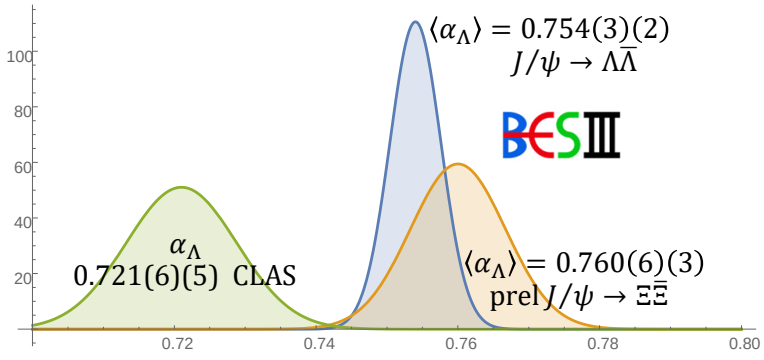


**Figure 6: Value of $\alpha_\Lambda$ decay parameter in $\Lambda \to p\pi^-$.** Comparison of two independent measurements of $\langle\alpha_\Lambda\rangle$ from BESIII [8, 10] and the CLAS determination of $\alpha_\Lambda$ [9].

The precision of the measurement in $J/\psi \to \Xi^-\overline{\Xi}^+$ is similar to that of the $J/\psi \to \Lambda\overline{\Lambda}$ study, despite a six times smaller data sample, primarily due to larger average polarization of $\Lambda$. This can be understood by recalling that even if $\Xi^-$ is unpolarized the $\Lambda$ from the $\Xi^- \to \Lambda\pi$ decay has longitudinal polarization equal to $|\alpha_\Xi| \approx 37\%$, while in $e^+e^- \to J/\psi \to \Lambda\overline{\Lambda}$ the average magnitude of the $\Lambda$ polarization vector is 19%.

### 6.2 Discussion of CP-violation tests

To compare the measurements of $A_{\rm CP}$ with the predictions for the weak-phase differences given in Table 1 a knowledge of the strong-phase difference $\delta^P - \delta^S$ is required. Since $A_{\rm CP}$ is proportional to $\tan(\delta^P - \delta^S)$, which is a small number, the experimental sensitivity to the weak-phase difference value and/or the precision of the prediction are decreased. For decay $\Lambda \to p\pi^-$ this factor can be determined using Eq. (18), where the $\delta_1^S = 0.11(2)$ and $\delta_1^P = -0.014(1)$ [53]. For decay $\Xi^- \to \Lambda\pi^-$ it is determined experimentally using the methods discussed in this contribution. Since the present result for $\beta_\Xi$ is consistent with zero the $A_{\rm CP}^\Xi$ value cannot be used to determine the weak-phase difference. However, the $B_{\rm CP}^\Xi$ measurement determines directly $\xi_P - \xi_S$ with good precision. The SM predictions for the weak phases are two orders of magnitude below the present uncertainties for $\Lambda$ and $\Xi$. The published HyperCP result [35] on the sum $A_{\rm CP}^\Lambda + A_{\rm CP}^\Xi$, interpreted by neglecting the $A_{\rm CP}^\Xi$ contribution, translates to $(\xi_P - \xi_S)_\Lambda = 0.000(5)$.

The CP-violation studies in hyperon decays are complementary to $\epsilon'/\epsilon$ measurement in kaons in two ways. The direct CP violation effects in kaon decays must involve both $|\Delta I| = 1/2$ $|\Delta I| = 3/2$ transition where the CP-odd phases come from the QCD, Fig. 1(c) and electroweak, Fig. 1(d), penguin contributions, respectively. There is a delicate balance and cancellation of the two contributions. In the hyperon decays the CP-violation signal mainly comes from $|\Delta I| = 1/2$ transitions and is dominated by the QCD penguins. Moreover, due to vector nature of gluons exchanges, one can expect a non-trivial helicity structure of the *sdg* vertices. In particular certain BSM mechanisms will only contribute to the spin observables accessible in the hyperon decays. One such scenario assuming effects dominated by chromomagnetic-penguin operators is discussed in Ref. [32], where a general relation between the hyperon weak-phase difference and kaon observables was derived:

$$(\xi_P - \xi_S)_{BSM} = \frac{C'_B}{B_G}\left(\frac{\epsilon'}{\epsilon}\right)_{BSM} + \frac{C_B}{\kappa}\epsilon_{BSM} \ . \tag{34}$$

The $C_B$ and $C'_B$ parameters are given in Table 2, $B_G$ parameterizes the hadronic uncertainty and $\kappa$ quantifies contribution of the different poles. The allowed range of $(\epsilon'/\epsilon)_{BSM}$ and $\epsilon_{BSM}$ can be estimated from a comparison of the experimental values of $\mathrm{Re}(\epsilon'/\epsilon)$ and $|\epsilon|$ with the recent SM predictions [54]:

$$-4\times10^{-4} \le \left(\frac{\epsilon'}{\epsilon}\right)_{BSM} \le 10^{-3} \ , \ |\epsilon|_{BSM} < 2\times10^{-4} \ . \tag{35}$$

Using $0.5 < B_G < 2$ and $0.2 < |\kappa| < 1$ [55], the kaon data put constraints on the weak-phase differences $\xi_P - \xi_S$ to $-7.9\times10^{-4} \le (\xi_P - \xi_S)^\Lambda_{BSM} \le 1.26\times10^{-3}$ and $-1.26\times10^{-3} \le (\xi_P - \xi_S)^\Xi_{BSM} \le 0.6\times10^{-3}$. A result in the hyperon sector with better sensitivity will provide an independent constraint for the BSM contributions to the CP violation in the strange quark sector. However, a lot remains to be done on the theory prediction side — the calculations were done twenty years ago and the coefficients in these relations have errors of 200%.

| | $\sigma(A_{\rm CP}^{\Lambda})$ | $\sigma(A_{\rm CP}^{\Xi})$ | $\sigma(B_{\rm CP}^{\Xi})$ | Comment |
|---|---|---|---|---|
| BESIII | $1.0\times10^{-2}(*)$ | $1.3\times10^{-2}$ | $3.5\times10^{-2}$ | $1.3\times10^{9}$ $J/\psi$ [8, 10] |
| BESIII | $3.6\times10^{-3}$ | $4.8\times10^{-3}$ | $1.3\times10^{-2}$ | $1.0\times10^{10}$ $J/\psi$ |
| SCTF | $2.0\times10^{-4}$ | $2.6\times10^{-4}$ | $6.8\times10^{-4}$ | $3.4\times10^{12}$ $J/\psi$ |

$(*)$ – the result is a combination of the two BESIII measurements

**Table 5: Projections of the expected statistical uncertainties for the hyperon CP-odd observables $A_{\rm CP}^{\Lambda}$, $A_{\rm CP}^{\Xi}$ and $B_{\rm CP}^{\Xi}$ with the full BESIII data set and at the SCTF colliders. The uncertainties are based on the statistical uncertainties in the BESIII measurements given in the first row [8, 10].**

## 7. Outlook: SCTF with polarized electron beam

The hyperon decay studies can be an important topic at next-generation electron–positron colliders — the presently discussed Super Charm-Tau Factories in Russia [56] and in China [57]. The design luminosity of $10^{35}$ cm$^{-2}$s$^{-1}$ will be two orders of magnitude larger than BEPCII, allowing for data samples of more than $10^{12}$ $J/\psi$ events. The projection of statistical uncertainties for the CP-odd observables are shown in Table 5, implying that the sensitivity will be close the SM predictions. To reduce further the uncertainties two additional improvements should be considered: (1) the c.m. energy spread $\Delta E$ reduction and (2) electron-beam longitudinal polarization. The c.m. spread in colliders such as BEPCII is determined by the radiative loses and $\Delta E$ at $J/\psi$ is ∼1.0 MeV. A collision scheme where electrons(positrons) with higher momenta are matched with positrons(electrons) with lower momenta promises $\Delta E$ reduction. Ultimately the reduction to match the $J/\psi$ width of 90 keV could provide an order of magnitude increase of the $J/\psi$ decay events for a given integrated luminosity [58–60]. However, it is not clear how much the instantaneous luminosity will be reduced in such scheme. Instead, I will discuss some implications for the hyperon CP-violation measurements with the longitudinally polarized electron beam, where the beam polarization of 80% at the $J/\psi$ energies can be obtained without reduction of the beam current [61].

The spin correlation matrix including the longitudinal electron beam polarization $P_e$ is

$$\frac{3}{3+\alpha_\psi}\cdot\begin{pmatrix} 1+\alpha_\psi\cos^2\theta & \gamma_\psi P_e\sin\theta & \beta_\psi\sin\theta\cos\theta & (1+\alpha_\psi)P_e\cos\theta \\ \gamma_\psi P_e\sin\theta & \sin^2\theta & 0 & \gamma_\psi\sin\theta\cos\theta \\ -\beta_\psi\sin\theta\cos\theta & 0 & \alpha_\psi\sin^2\theta & -\beta_\psi P_e\sin\theta \\ -(1+\alpha_\psi)P_e\cos\theta & -\gamma_\psi\sin\theta\cos\theta & -\beta_\psi P_e\sin\theta & -\alpha_\psi-\cos^2\theta \end{pmatrix}, \tag{36}$$

The $B$-baryon polarization vector $\mathbf{P}_B$ defined in the rest frame of baryon $B$ is:

$$\mathbf{P}_B = \frac{\gamma_\psi P_e\sin\theta\hat{\mathbf{x}}_1 - \beta_\psi\sin\theta\cos\theta\hat{\mathbf{y}}_1 - (1+\alpha_\psi)P_e\cos\theta\hat{\mathbf{z}}_1}{1+\alpha_\psi\cos^2\theta}\,. \tag{37}$$

In Fig. 7 the magnitude of the $\Lambda$ polarization as a function of $\cos\theta$ in $e^+e^-\to J/\psi\to\Lambda\overline{\Lambda}$ is drawn assuming three different values of the electron beam polarization. Average value of the baryon polarization vector squared $\langle\mathbf{P}_B^2\rangle$, defined as

$$\langle\mathbf{P}_B^2\rangle = \int\mathbf{P}_B^2\left(\frac{1}{\sigma}\frac{{\rm d}\sigma}{{\rm d}\Omega_B}\right){\rm d}\Omega_B\,, \tag{38}$$

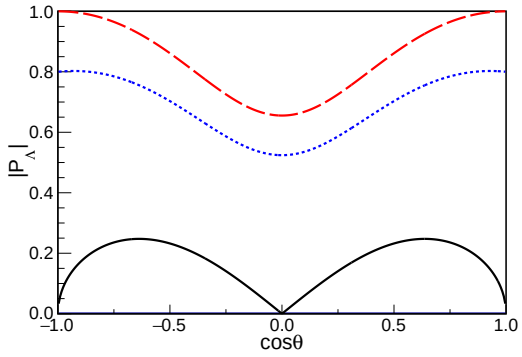


**Figure 7: Spin polarization of $\Lambda$ in $e^+e^- \to J/\psi \to \Lambda\overline{\Lambda}$ with polarized electron beam.** Magnitude of the $\Lambda$ polarization vector as a function of the production angle for the electron beam polarizations $P_e = 0$, 0.8, 1 (solid, dotted, dashed lines, respectively). The $\alpha_\psi$ and $\Delta\Phi$ are taken as the central values measured by BESIII given in Table 3.

determines the statistical uncertainty of the $A_{\rm CP}$. It can be approximately expressed as

$$\sigma(A_{\rm CP}^D) \approx \frac{1}{\alpha_D}\sqrt{\frac{3}{2}}\frac{1}{\sqrt{N}}\sqrt{\frac{1}{\langle \mathbf{P}_B^2\rangle}}\,. \tag{39}$$

The average polarizations squared $\langle \mathbf{P}_B^2\rangle$ are linear functions of the electron beam polarization squared

$$\langle \mathbf{P}_B^2\rangle = c_0 + c_2 P_e^2\,, \tag{40}$$

where the coefficients $c_0$ and $c_2$ depend on the $\alpha_\psi$ and $\Delta\Phi$ parameters. In Fig. 8(a) the average polarizations are shown for the $\Lambda$, $\Sigma^+$ and $\Xi^-$ baryons from the $J/\psi$ decays using the values of the parameters from Table 3. Figure 8(b) shows statistical uncertainties for $A_{\rm CP}^\Lambda$ and $A_{\rm CP}^\Sigma$, multiplied by $\sqrt{N}\alpha_D$ as a function of $P_e$, where solid lines represent the exact numerical calculations and dashed lines represent the approximation from Eq. (39). Therefore electron-beam polarization of 80% reduces the uncertainty for $A_{\rm CP}^\Lambda$ four times comparing to the use of unpolarized beams. Without the polarization such improvement would require to use 16 times more events. The improvement is even more dramatic for the $\Sigma^+$ baryon. The numerical result given by red-solid line is for the $\Sigma p(\Sigma^+ \to p\pi^0)$ decay where $\alpha_{\Sigma p} \approx -1$, while the red-dashed line describes both the approximation and the exact result for $\Sigma n(\Sigma^+ \to n\pi^+)$ with $\alpha_{\Sigma n} \approx 0$.

## 8. Acknowledgements

This work was supported in part by National Natural Science Foundation of China (NSFC) under Contract No. 11935018., Polish National Science Centre through the Grant 2019/35/O/ST2/02907 and by the CAS President's International Fellowship Initiative (PIFI).

## References

[1] Dubnickova A Z, Dubnicka S and Rekalo M P 1996 *Nuovo Cim.* **A109** 241–256

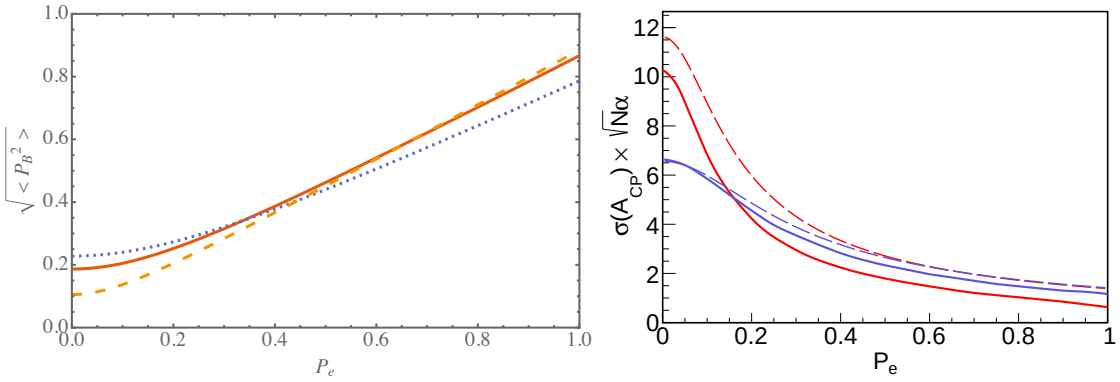


**Figure 8: Baryon average polarization and $A_{\rm CP}$ sensitivity as a function of electron beam polarization** $P_e$ (left) average polarization squared for $\Lambda$ (line), $\Xi^-$ (dotted line) and $\Sigma^+$ (dashed line). (right) Sensitivities of the $A_{\rm CP}$ measurement times the decay parameter value for (blue) $\Lambda$ and (red) $\Sigma^+$. The dashed lines correspond to the approximation from Eq. (39).


[2] Gakh G I and Tomasi-Gustafsson E 2006 *Nucl. Phys.* **A771** 169–183

[3] Czyz H, Grzelinska A and Kuhn J H 2007 *Phys. Rev.* **D75** 074026

[4] Fäldt G 2015 *Eur. Phys. J.* **A51** 74

[5] Fäldt G 2016 *Eur. Phys. J.* **A52** 141

[6] Fäldt G and Kupsc A 2017 *Phys. Lett.* **B772** 16–20

[7] Tanabashi M *et al.* (Particle Data Group) 2018 *Phys. Rev. D* **98** 030001

[8] Ablikim M *et al.* (BESIII) 2019 *Nature Phys.* **15** 631–634

[9] Ireland D G, Döring M, Glazier D I, Haidenbauer J, Mai M, Murray-Smith R and Rönchen D 2019 *Phys. Rev. Lett.* **123** 182301

[10] Ablikim M *et al.* (BESIII) 2021 (*Preprint* 2105.11155)

[11] Ablikim M *et al.* (BESIII) 2020 *Phys. Rev. Lett.* **125** 052004

[12] Huang M *et al.* (HyperCP) 2004 *Phys. Rev. Lett.* **93** 011802

[13] Ablikim M *et al.* (BESIII) 2021 *Phys. Rev. Lett.* **126** 092002

[14] Lee T D, Steinberger J, Feinberg G, Kabir P K and Yang C N 1957 *Phys. Rev.* **106** 1367–1369

[15] Overseth O E and Pakvasa S 1969 *Phys. Rev.* **184** 1663–1667

[16] Lee T D and Yang C N 1957 *Phys. Rev.* **108** 1645–1647

[17] Perotti E, Fäldt G, Kupsc A, Leupold S and Song J J 2019 *Phys. Rev.* **D99** 056008

[18] Batley J R *et al.* (NA48) 2002 *Phys. Lett. B* **544** 97–112

[19] Alavi-Harati A *et al.* (KTeV) 2003 *Phys. Rev. D* **67** 012005 [Erratum: Phys.Rev.D 70, 079904 (2004)]

[20] Abouzaid E *et al.* (KTeV) 2011 *Phys. Rev. D* **83** 092001

[21] Wolfenstein L 1964 *Phys. Rev. Lett.* **13** 562–564

[22] Buras A 2020 *Gauge Theory of Weak Decays* (Cambridge University Press) ISBN 978-1-139-52410-0, 978-1-107-03403-7

[23] Bai Z *et al.* (RBC, UKQCD) 2015 *Phys. Rev. Lett.* **115** 212001

[24] Abbott R *et al.* (RBC, UKQCD) 2020 *Phys. Rev. D* **102** 054509

[25] Gisbert H and Pich A 2018 *Rept. Prog. Phys.* **81** 076201

[26] Cirigliano V, Gisbert H, Pich A and Rodríguez-Sánchez A 2020 *JHEP* **02** 032

[27] Aebischer J, Bobeth C and Buras A J 2020 *Eur. Phys. J. C* **80** 705

[28] Bigi I I and Sanda A I 2009 *CP violation* vol 9 (Cambridge University Press) ISBN 978-0-511-57728-4, 978-0-521-84794-0, 978-1-107-42430-2

[29] Donoghue J F and Pakvasa S 1985 *Phys. Rev. Lett.* **55** 162

[30] Pais A 1959 *Phys. Rev. Lett.* **3** 242–244

[31] Tandean J and Valencia G 2003 *Phys. Rev.* **D67** 056001

[32] Tandean J 2004 *Phys. Rev. D* **69** 076008

[33] Zyla P A *et al.* (Particle Data Group) 2020 *PTEP* **2020** 083C01

[34] White C G *et al.* 1999 *Nucl. Phys. B Proc. Suppl.* **71** 451–456

[35] Holmstrom T *et al.* (HyperCP) 2004 *Phys. Rev. Lett.* **93** 262001

[36] Materniak C (HyperCP) 2009 *Nucl. Phys. B Proc. Suppl.* **187** 208–215

[37] Ablikim M *et al.* (BESIII) 2017 *Phys. Rev. D* **95** 052003

[38] Ablikim M *et al.* (BES) 2008 *Phys. Rev. D* **78** 092005

[39] Ablikim M *et al.* (BESIII) 2017 *Phys. Lett. B* **770** 217–225

[40] Hiesmayr B C 2015 *Sci. Rep.* **5** 11591

[41] Harris F, Overseth O E, Pondrom L and Dettmann E 1970 *Phys. Rev. Lett.* **24** 165–168

[42] Bellamy E H *et al.* 1972 *Phys. Lett. B* **39** 299–302

[43] Lipman N H *et al.* 1973 *Phys. Lett. B* **43** 89–92

[44] Aubert B *et al.* (BaBar) 2006 *Phys. Rev. Lett.* **97** 112001

[45] Korner J G and Kuroda M 1977 *Phys. Rev. D* **16** 2165

[46] Doncel M G, Michel L and Minnaert P 1972 *Nucl. Phys. B* **38** 477–528

[47] Aaij R *et al.* (LHCb) 2015 *Phys. Rev. D* **92** 011102

[48] Tandean J 2004 *Phys. Rev. D* **70** 076005

[49] Chen Y C *et al.* (HyperCP) 2005 *Phys. Rev. D* **71** 051102

[50] Lu L C *et al.* (HyperCP) 2005 *Phys. Lett. B* **617** 11–17

[51] Lu L C *et al.* (HyperCP) 2006 *Phys. Rev. Lett.* **96** 242001

[52] Adlarson P and Kupsc A 2019 *Phys. Rev. D* **100** 114005

[53] Hoferichter M, Ruiz de Elvira J, Kubis B and Meißner U G 2016 *Phys. Rept.* **625** 1–88

[54] Aebischer J, Buras A J and Kumar J 2020 *JHEP* **12** 097

[55] He X G, Murayama H, Pakvasa S and Valencia G 2000 *Phys. Rev. D* **61** 071701

[56] Levichev E B, Skrinsky A N, Tumaikin G M and Shatunov Y M 2018 *Phys. Usp.* **61** 405–423

[57] Luo Q and Xu D 2018 Progress on Preliminary Conceptual Study of HIEPA, a Super Tau-Charm Factory in China *9th International Particle Accelerator Conference*

[58] Renieri A 1975 Possibility of Achieving Very High-Energy Resolution in electron-Positron Storage Rings LNF-75/6-R

[59] Avdienko A A, Kornyukhin G A, Protopopov I Y, Skrinsky A N, Temnykh A B, Tumaikin G M and Zholents A A 1983 *Conf. Proc. C* **830811** 186–189

[60] Telnov V I 2020 Monochromatization of $e^+e^-$ colliders with a large crossing angle (*Preprint* 2008.13668)

[61] Koop I, Bogomyagkov A and Otboev A 2019 Longitudinal Polarization in Novosibirsk c-tau factory *2019 Joint Workshop on Future charm-tau Factory* URL https://c-tau.ru/indico/event/3/contributions/206/